Structure of the EGF receptor transactivation circuit integrates multiple signals with cell context†

Elizabeth J. Joslin,‡[a] Harish Shankaran,‡[b] Lee K. Opresko,[b] Nikki Bollinger,[b] Douglas A. Lauffenburger[a] and H. Steven Wiley*[bc]

Received 5th March 2010, Accepted 21st April 2010
First published as an Advance Article on the web 10th May 2010
DOI: 10.1039/c003921g

Transactivation of the epidermal growth factor receptor (EGFR) is thought to be a process by which a variety of cellular inputs can be integrated into a single signaling pathway through either stimulated proteolysis (shedding) of membrane-anchored EGFR ligands or by modification of the activity of the EGFR. As a first step towards building a predictive model of the EGFR transactivation circuit, we quantitatively defined how signals from multiple agonists were integrated both upstream and downstream of the EGFR to regulate extracellular signal regulated kinase (ERK) activity in human mammary epithelial cells. By using a "non-binding" reporter of ligand shedding, we found that transactivation triggers a positive feedback loop from ERK back to the EGFR such that ligand shedding drives EGFR-stimulated ERK that in turn drives further ligand shedding. Importantly, activated Ras and ERK levels were nearly linear functions of ligand shedding and the effect of multiple, sub-saturating inputs was additive. Simulations showed that ERK-mediated feedback through ligand shedding resulted in a stable steady-state level of activated ERK, but also showed that the extracellular environment can modulate the level of feedback. Our results suggest that the transactivation circuit acts as a context-dependent integrator and amplifier of multiple extracellular signals and that signal integration can effectively occur at multiple points in the EGFR pathway.

Introduction

Mounting evidence over the past decade indicates that the EGFR pathway can be activated indirectly by numerous, diverse stimuli in the extracellular environment.[1–4] This phenomenon of receptor transactivation can be elicited by other growth factors, ligands for G-protein coupled receptors, steroid hormones, the extracellular matrix, pathogens, and mechanical force,[5] and has been observed in a wide variety of cell types including breast, kidney, lung, dermal epithelial cells, smooth muscle cells, vascular endothelial cells, and cardiomyocytes.[6–8] Because of the ubiquity of EGFR transactivation phenomena, a high-level role has been proposed: that this circuit represents a mechanism by which information provided by diverse stimuli can be integrated to generate a more comprehensive, unified flux of signals through downstream signaling networks, especially the canonical Ras–Raf–ERK pathway.[4,9] This is an appealing concept for its potentially powerful contribution to understanding how cell phenotypic behavior is governed in a physiological context.

The ability of the EGFR pathway to integrate multiple cellular inputs has been postulated to be the primary reason why anti-EGFR antibodies and kinase inhibitors are so effective in treating diseases, such as cancer.[10] Because it integrates signals from multiple pathways, blocking this pathway should be more effective than trying to block individual pathways. However, the effect of blocking the EGFR on the response of cells should depend on the degree to which this pathway contributes to the action of a particular stimulus. Thus, predicting the therapeutic effect of blocking the EGFR pathway requires a quantitative understanding of the "transactivation circuit" and how different receptor pathways are coupled into it.

The most prominently described transactivation mechanism is regulated release of soluble EGFR ligands *via* proteolysis of transmembrane precursors.[11] Interestingly, these precursors are actually a family of ligands—EGF, transforming growth factor alpha (TGFα), amphiregulin, heparin-binding EGF-like growth factor, betacellulin, and epiregulin. Each exhibits disparate molecular characteristics related to receptor binding, endocytic trafficking, and interactions with other cell membrane and extracellular matrix components.[12] Although the data are not comprehensive, the particular ligands involved in transactivation appear to vary with the original stimulus.[13]

Along with the pursuit of increased detail concerning the molecular mechanisms of transactivation, a primary issue that needs to be addressed is the dynamic operation of the circuit as a whole. If this system indeed functions to integrate multiple

[a] *Department of Biological Engineering, Massachusetts Institute of Technology, Cambridge, MA 02139, USA*
[b] *Systems Biology Program, Pacific Northwest National Laboratory, Richland, WA 99354, USA. E-mail: steven.wiley@pnl.gov; Fax: +1 509-371-6354; Tel: +1 509-371-6551*
[c] *Environmental Molecular Sciences Laboratory, Pacific Northwest National Laboratory, Richland, WA 99354, USA*
† Electronic supplementary information (ESI) available: Supplemental methods and additional figures and tables. See DOI: 10.1039/c003921g
‡ These authors contributed equally to this manuscript.

diverse cell inputs into a single downstream signaling network, we need to discern the logic of this integration. For instance, autocrine ligand shedding is required to activate ERK in many circumstances,[14,15] but other reports have shown that ERK activation is required for shedding itself.[16–18] This challenging paradox could potentially arise from the presence of recursive feedback, alternative mechanisms regulating ligand release, or simple differences among the processes that regulate release in various cell types. However, these diverse possible explanations must be resolved in order to elucidate a systematic model for the EGFR transactivation circuit.

In this study, we delineated the regulatory logic of EGFR transactivation to the degree necessary to construct an internally consistent model of the overall process. To achieve this, we successfully addressed two technical issues that have limited previous efforts. The first issue is the different mechanisms by which multiple receptor systems can be coupled to the ERK pathway in different cells. It is very difficult to understand the overall system architecture based on data generated using diverse cell types. Thus, we have used a single, well-characterized human cell type (mammary epithelial cell) that requires activation of the EGF receptor system for proliferation both *in vitro* and *in situ*.[19] The second issue is the recursive nature of autocrine signaling, in which released ligands bind back to the producing cells, potentially stimulating further ligand release, thus rendering interpretation of data highly ambiguous. To enable quantitative analysis of ligand shedding, we have developed a "non-binding" ligand that can be shed in a normal fashion but cannot bind back and stimulate further release. This allowed us to isolate the effect of different signaling pathways on the rate of ligand shedding and thus to build a model of the overall process.

Rather than trying to define all of the molecular mechanisms involved in the transactivation process, we focused more on systems level processes. We defined the logical network for EGFR transactivation using a number of diverse stimuli including lysophosphatidic acid (LPA), hepatocyte growth factor (HGF), and EGF family ligands. We found that at physiological ligand levels, each of these stimuli act as linear inputs to an invariant TGFα–EGFR–Ras–ERK feedback circuit that produces a downstream ERK signal that integrates the various inputs. We then constructed a model of the transactivation circuit using a transfer function-based approach. This allowed us to explore the design principles of this circuit and show that the level of ERK induced by the feedback part of the circuit is dependent on cell context.

Results and discussion

The autocrine circuit is recursive

Previous investigations of EGFR transactivation have postulated that stimulated ligand shedding is the primary mechanism that is involved. These studies have been mostly qualitative because of the difficulty of measuring small amounts of released ligand and its rapid receptor-mediated uptake by cells. To quantify the rate of ligand shedding, we created a very sensitive reporter by fusing the receptor-binding domain of EGF to the membrane-anchoring domain of TGFα.[20] This ligand, which we term TCT (TGFα Cytoplasmic Tail), is efficiently expressed by human mammary epithelial cells (HMEC) and is released into the medium (Fig. 1A). This ligand chimera has the strong advantage of allowing us to use an extremely sensitive EGF ELISA to quantify ligand shedding, even in the presence of large amounts of added TGFα.[21] Since HMEC do not express EGF endogenously, the EGF ELISA allows us to directly measure the amount of TCT shed by the cells.

Inhibiting cell surface metalloproteases with batimastat[22] completely prevented soluble ligand from appearing in the medium, confirming its production by proteolytic shedding (Fig. 1A). When we prevented cells from consuming this released ligand by blocking the EGFR with an antagonistic antibody (225mAb), however, we paradoxically saw a decrease in detectable ligand (Fig. 1A) suggesting that EGFR activation was stimulating ligand release. In support of this idea, inhibiting EGFR kinase activity using the small molecule inhibitor gefitinib also strongly reduced ligand production (Fig. 1B). These results are consistent with previous reports that TGFα can stimulate its own proteolytic release through activation of the EGFR.[23]

It has previously been shown that released EGFR ligands will stimulate activation of the ERK cascade.[5,20] Further, activated ERK has been postulated to be required for ligand shedding.[16,17] Blocking ERK activation with the inhibitor PD98059 did indeed greatly inhibit ligand release, but the p38 inhibitor SB203580 had little effect (Fig. 1B), indicating that regulated ligand release is specifically driven by activation of the ERK pathway. It also indicates that activation of the EGFR by released autocrine ligands drives further ligand release by activating the ERK pathway.

The ability of TCT to be both consumed by cells and conversely induce further TCT release greatly complicates efforts to quantify individual aspects of the pathway. To circumvent this problem, we generated a "no-affinity" version of TCT (termed "TCT-NA") by a L-to-G substitution at EGF position 15. This has previously been shown to reduce the affinity of EGF for its receptor by $>99\%$ without altering ligand structure.[24] To prevent a potential saturation of the proteolytic processing system, the TCT-NA ligand was expressed at less than the endogenous level of amphiregulin, which is the primary ligand made by HMEC.[25] We found that the shedding of TCT-NA was inhibited by batimastat treatment (Fig. 1C), but not by blocking the EGFR (Fig. 1D). Because of its low affinity, TCT-NA exhibited $<3\%$ of the effective biological activity of TCT, as measured by its ability to stimulate phosphorylation of the EGFR (Fig. 1E). Importantly, the ability of a panel of agonists to stimulate the release of TCT-NA is virtually identical to that observed for the endogenous EGFR ligand amphiregulin (Fig. S1, ESI†). These data show that TCT-NA is a suitable reporter ligand for quantifying the regulated release of EGFR ligands in HMEC.

When cells expressing TCT-NA were stimulated with TGFα, there was a strong initial stimulation of ligand release, followed by an approach to a steady state by 6 hours (Fig. 1F). This stimulated release was completely blocked by inhibiting the ERK pathway with PD98059, but the constitutive rate

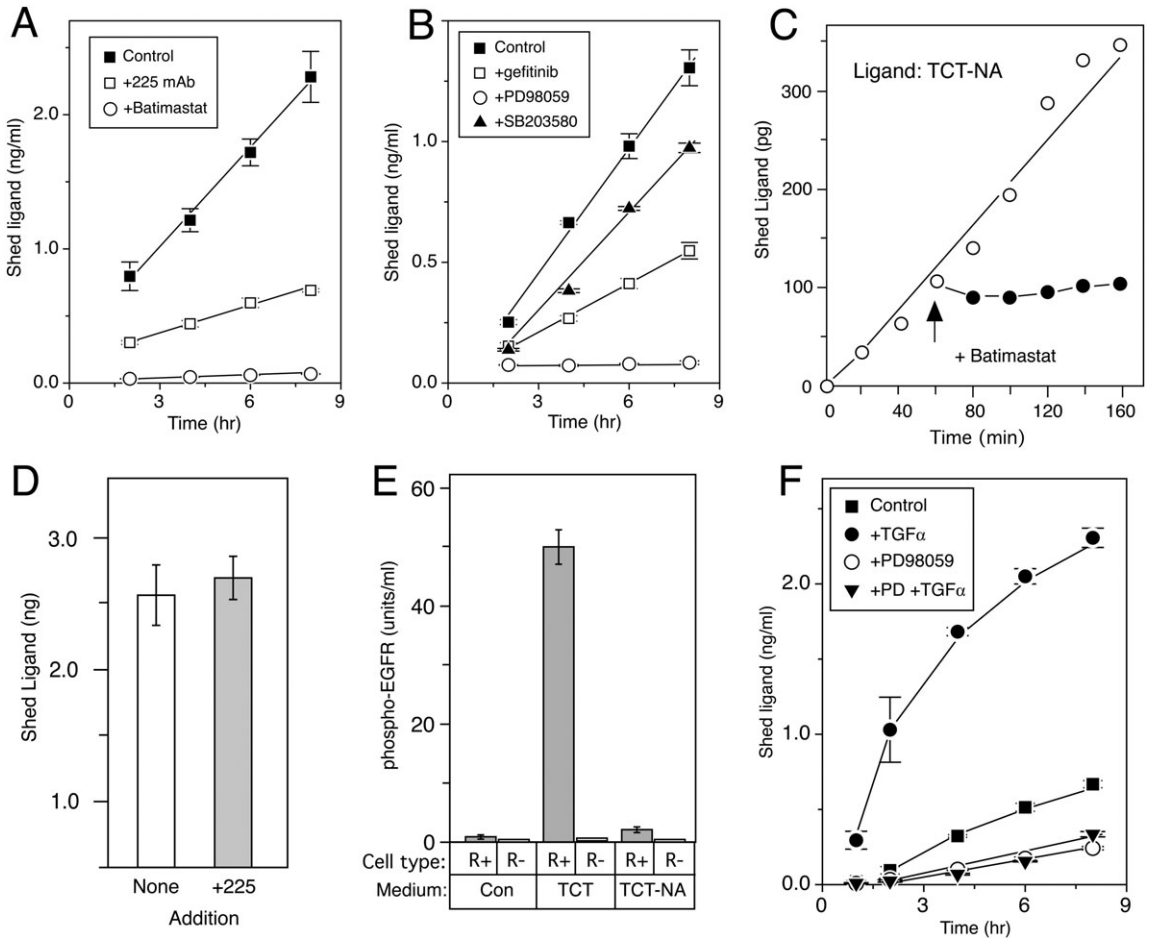

Fig. 1 EGFR autocrine ligands stimulate their own release by activating ERK. (A) Accumulation of EGF in medium is inhibited by blocking the EGFR or inhibiting cell surface proteolysis. After 16 hours in serum-free media, cells expressing the chimeric ligand TCT were switched to fresh serum-free media alone or containing 10 μg ml^{-1} 225mAb or 225mAb in addition to 10 μM batimastat. Media from triplicate wells was collected at 2 hour intervals, assayed for EGF with an ELISA. Error bars represent standard deviation. (B) Effects of inhibitors on ligand release. After 16 hours in serum-free media, TCT cells were pre-incubated with the indicated inhibitors for 30 minutes. Cells were then switched to either fresh serum-free media alone (control) or containing 1 μM gefitinib, 10 μM SB203580 or 25 μM PD98059. Other conditions same as A. (C) Cells expressing TCT-NA were switched to fresh serum-free medium at $t = 0$, and the amount of immunoreactive EGF in the medium was determined by ELISA (open circles). At 1 h, batimastat was added to a final concentration of 10 μM to a parallel set of cells (closed circles). (D) Blocking the EGFR has no significant effect on release of TCT-NA. Cells expressing TCT-NA were changed to serum-free medium either in the absence (open bars) or presence (closed bars) of 10 μg ml^{-1} of 225mAb. After 8 h, the medium was collected and the concentration of immunoreactive EGF was measured by ELISA. Error bars are SD from triplicate wells. (E) TCT-NA fails to activate the EGFR. Serum-free conditioned medium was collected from an overnight incubation of WT HMEC (control medium) or from cells expressing either TCT or TCT-NA. Immunoreactive levels of EGF were determined by ELISA and the final concentrations of both ligands were adjusted to 5 ng ml^{-1}. Parental B82 mouse fibroblasts lacking the EGFR (R−) or transfected with the human EGFR (R+) were incubated with the indicated medium for 10 min. The levels of phospho-EGFR were measured by ELISA. Error bars are SD from triplicate wells. (F) Shedding of the non-bindable EGFR ligand TCT-NA is stimulated by TGFα and inhibited by ERK inhibitors. After 16 hours in serum-free media, cells were switched to fresh serum-free media alone or medium containing 20 ng ml^{-1} TGFα, both in the presence or absence of 25 μM PD98059. Other conditions same as A.

of release was only reduced by about 50% (Fig. 1F). The p38 pathway does not appear to be involved in stimulated ligand release because inhibiting this pathway using SB203580 only caused a small decrease in stimulated shedding, likely due to its effect on constitutive release (Fig. S2, ESI†). This finding is consistent with previous observations regarding regulated shedding and the important role of the ERK pathway in this process.[16,17] However, it does not address the fundamental paradox of how ERK can be necessary for ligand shedding when ligand shedding is necessary for ERK.

ERK-stimulated ligand shedding displays a temporal delay

Previously, we have demonstrated that the ERK pathway can be activated in HMEC by three distinct mechanisms: (1) directly through the EGFR by TGFα addition, (2) indirectly through the EGFR by stimulated ligand release (transactivation) and (3) independently of the EGFR through the HGF/MET pathway.[25] To determine whether ligand shedding can be temporally separated from ERK activation, we stimulated the ERK pathway through these three distinct mechanisms by the addition of TGFα, LPA and HGF

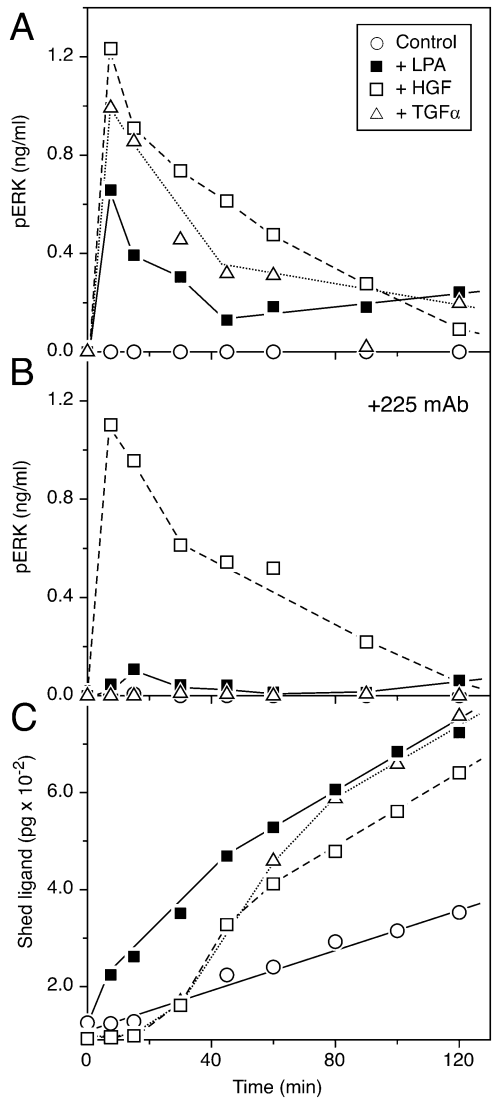

Fig. 2 Kinetics of ERK activation and induced shedding. (A) Kinetics of ERK phosphorylation using 3 ng ml^{-1} TGFα, 3 μM LPA or 20 ng ml^{-1} HGF as stimulants. Cells were seeded at 350 000 cells per 6-well dish on day 1 and shifted into serum-free medium (DFB) on day 2. Following an 18 hour incubation, ligand was added for the indicated time at which point cell lysates were collected and assayed for pERK by ELISA as described in Experimental. (B) Same as A, but cells were first pretreated for 1 h with 10 μg ml^{-1} 225mAb to block the EGFR. (C) Kinetics of shedding of cells expressing TCT-NA using the same conditions as A except that cells were washed in DFB and then placed in 1 ml of fresh DFB +/− stimulus. The medium was then collected at the indicated times. The results are the average of two independent experiments.

respectively. The levels of phosphorylated ERK (pERK) were measured using a quantitative ELISA because we have found this assay more quantitative and robust than Western-based assays.[25] As shown in Fig. 2A, addition of any of these three agonists caused a rapid (<10 min) peak in ERK phosphorylation followed by a gradual decline to steady state by 2 h. There were no obvious qualitative differences in the time course profiles of ERK activation between the three agonists. However, blocking the EGFR with 225mAb inhibited ERK activation in the case of LPA and TGFα, but had no effect on HGF activity (Fig. 2B). Moreover, when the kinetics of induced shedding was examined, we observed that LPA caused an immediate increase in ligand shedding whereas there was a delay of ~20 minutes for shedding when the ERK pathway was stimulated by either TGFα or HGF (Fig. 2C). This temporal difference suggests that although ERK activity might be required for stimulated shedding, it does not directly stimulate cell surface proteolysis.

The most likely mechanism for the delay in ERK-induced shedding is that ERK activity enhances the transport of shedding proteases to the cell surface. We have previously shown that the protease in HMEC responsible for ligand shedding is ADAM17[25] and ERK activation accelerates its exit from the endoplasmic reticulum and transport to the cell surface.[26] Significantly, the reported kinetics of this stimulated transport is consistent with the time delay we observe for increased shedding following ERK activation. The rapidity of LPA-induced shedding, in contrast, suggests that it operates directly at the cell surface through an independent mechanism.

Sequence of biochemical pathways in the transactivation circuit

As a first step in dissecting the transactivation circuit, we used a panel of inhibitors to determine which signaling pathways were associated with each agonist (see Table S1 in the ESI†). Pathways shared by the different agonists should show up as sensitivity to the same inhibitors whereas distinct sensitivities should indicate agonist-specific pathways. When we measured the ability of different inhibitors to block LPA, TGFα or HGF-stimulated ERK phosphorylation, we found that MEK inhibitors were the only ones that could effectively block all three (Table S1, ESI†). PI3K inhibitors blocked HGF-stimulated ERK activation, consistent with previous studies.[27] EGFR inhibitors diminished both LPA and TGFα-stimulated ERK, in agreement with our previous data (Fig. 2B; also see ref. 25). To ascertain which LPA-stimulated pathways reside upstream of the EGFR, we looked for inhibitors that blocked LPA-induced, but not TGFα-induced ERK phosphorylation. These included Src, PI3K and IKK inhibitors (Table S1, ESI†). Surprisingly, most inhibitors had little effect on ERK activation stimulated by any agonist, including those against PKA, PKC, JAK2, JNK and p38-MAPK, suggesting that only a limited number of signaling pathways directly feed into the EGFR transactivation circuit.

To establish the logical relationship between shedding and ERK activation, we simultaneously measured shedding and the level of phosphorylated ERK (pERK) activation as a function of the concentration of different inhibitors. As shown in Fig. 3A, increasing amounts of U0126, a MEK inhibitor, effectively blocked pERK stimulated by both LPA and TGFα at the same dose. In contrast, U0126 was relatively selective in blocking TGFα *versus* LPA-induced shedding. Conversely, PP2, a Src kinase family inhibitor, was very efficient in blocking both LPA and TGFα-induced shedding, but was much more effective in inhibiting LPA *versus* TGFα-induced pERK (Fig. 3B). The results for the PI3K inhibitor LY294002 (Fig. S3, ESI†) were similar to those obtained for PP2. The EGFR inhibitor PD-153035 was also very effective in blocking

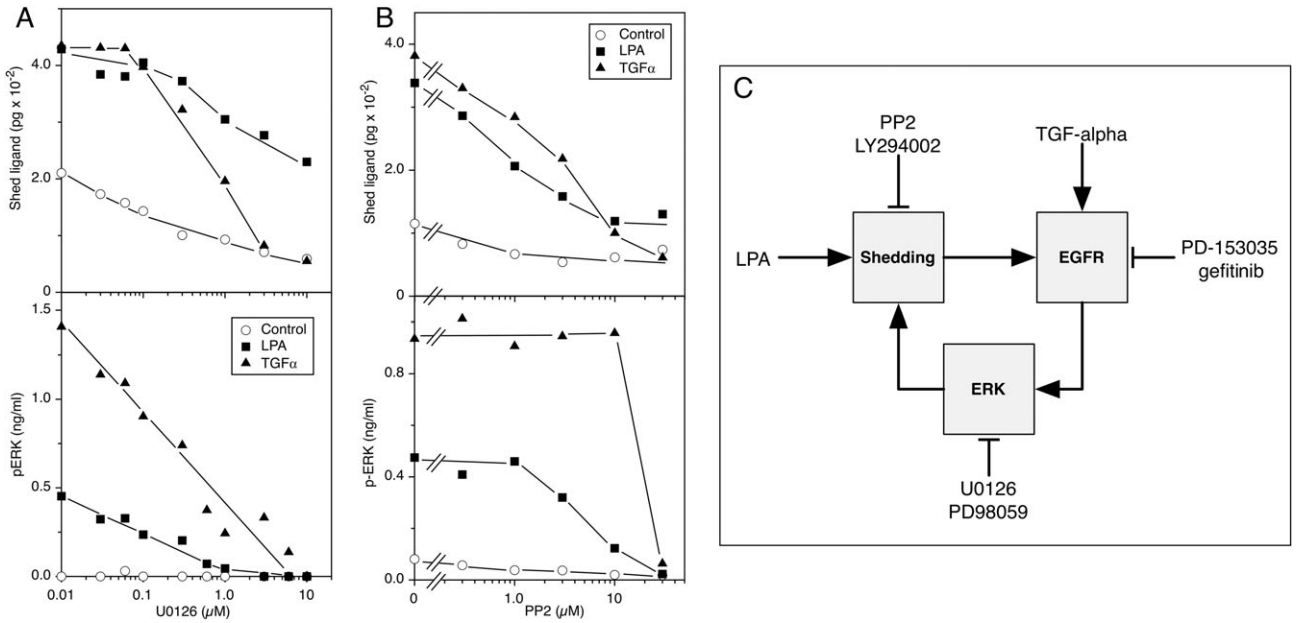

Fig. 3 Differential effect of inhibitors on shedding and ERK phosphorylation. (A) Inhibiting MEK blocks TGFα-stimulated shedding and ERK, but only blocks LPA-stimulated ERK. Upper panel—cells expressing TCT-NA (840K per well) were changed to serum-free medium overnight before a 1 h treatment within the indicated concentration of U0126. LPA (0.5 μM) or TGF (2.5 ng ml^{-1}) was added in a small aliquot (20 μL) and the cells incubated for an additional 90 min prior to collecting the medium and measuring the level of immunoreactive EGF by ELISA. Bottom panel—same as in top panel except that the cells were treated 10 min with agonists after which they were rinsed in ice-cold saline and lysed in detergent as described in Experimental. The levels of pERK were then measured by ELISA. (B) Inhibiting Src blocks both TGFα and LPA-induced shedding, but only inhibits LPA-stimulated ERK. Conditions same as A except that PP2 was used as the inhibitor and the cells were incubated with agonists for 15 min before measuring the levels of pERK by ELISA. (C) Relationships between effects of different inhibitors. The inhibitors are associated with the processes that are preferentially blocked.

TGFα-stimulated pERK, but had no effect on LPA-stimulated shedding, even at concentrations up to 1 μM (data not shown). The relative ability of the inhibitors to block ERK activation *versus* shedding can be arranged in the logical sequence shown in Fig. 3C.

The inhibitor data suggest that LPA and ERK activity act as independent inputs into the shedding process, and that TGFα and HGF each stimulate shedding through their ability to stimulate ERK. Moreover, the kinetic data (Fig. 2C) indicate that the ERK input exhibits a time delay relative to the direct effect of LPA. These findings raise the question of how the various inputs are quantitatively combined into a net ERK signal. To address this question, we quantified the relationship between the different inputs and measurable outputs, such as pERK levels and shedding rates.

Cells were treated with different concentrations of LPA and the rates of ligand shedding and levels of pERK were both measured. As shown in Fig. 4A, both measured outputs displayed an identical dependence on LPA concentration. Plotting the rate of ligand shedding against the levels of pERK resulted in a nearly linear relationship, indicating that the levels of activated ERK are directly proportional to the stimulated rate of ligand shedding. This apparent linearity arises despite the nonlinear, hyperbolic relationship between shedding and phospho-EGFR that we have described for this system;[20] also data not shown.

This surprising linear proportionality led us to ask whether inputs entering the transactivation circuit at other nodes exhibit similar behavior. A well-established nexus where other receptor systems join the ERK cascade is Ras activation. For example, HGF is known to stimulate Ras through a Gab1/Shp2 complex[28] whereas the EGFR uses a Shc/Grb2/SOS pathway.[29] To determine whether pERK activity is directly proportional to Ras activity, we treated cells with different concentrations of TGFα and then simultaneously measured these two quantities. As shown in Fig. 4B, the levels of activated Ras and pERK coordinately increased as a function of TGFα concentration. A slight decrease in both was seen at high TGFα concentrations, likely due to endocytic downregulation of surface EGFR,[30] but across all TGFα concentrations pERK levels were directly proportional to the activated Ras levels, indicating similar linear pathway behavior at the Ras signaling node.

To determine whether linearity of the ERK pathway was maintained during its feedback effect on ligand shedding, we varied pERK levels by adding increasing concentrations of TGFα, or by adding increasing amounts of the MEK inhibitor PD98059 together with a high concentration of TGFα. We then measured the pERK levels at 2 h together with the rates of ligand shedding. As shown in Fig. 5A, the amount of ligand shedding was directly proportional to pERK levels regardless of whether the pERK levels were modulated by increasing TGFα stimulation or by decreasing MEK activity.

To determine whether the amount of shed ligand was proportional to the level of pERK independent of the primary stimulus, we reexamined the data in Fig. 3A that shows the

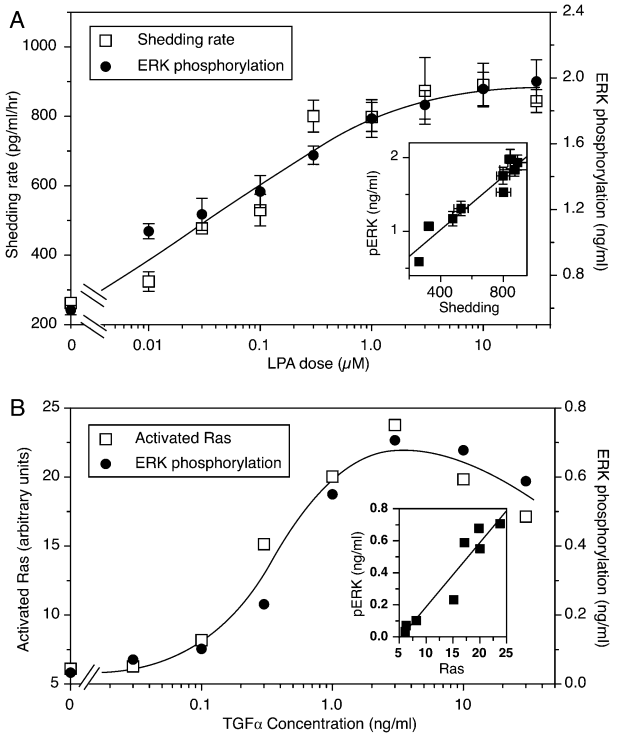

Fig. 4 Primary signaling nodes in transactivation circuit are linearly coupled. (A) ERK activation is directly proportional to LPA-induced shedding. Cells expressing TCT-NA (825K per well) were switched to 900 μl fresh medium for 1 h and then brought to the indicated concentrations of LPA using 100 μl of stock. After an additional hour, the medium was collected and the levels of immunoreactive EGF were measured using an ELISA. Data are average of duplicate experiments. Parallel plates of HMEC were stimulated with LPA for 5 minutes and then cell lysates were collected and measured for pERK using an ELISA. Data are average of replicate samples. Inset: shed ligand plotted against pERK levels. Units are same as main figure and line is from linear regression. (B) ERK activation is proportional to Ras activation. Cells were plated at a density of 6×10^6 cells per 150 mm plates and grown for 24 h. After shifting to DFB medium overnight, cells were stimulated with the indicated concentrations of TGFα for 15 min and lysates were collected for the Ras assay as described in the Experimental. The same lysates were used to measure pERK levels by ELISA. The results are the average of three experiments. Inset: the levels of activated Ras and pERK at each TGFα concentration. Units are same as main figure.

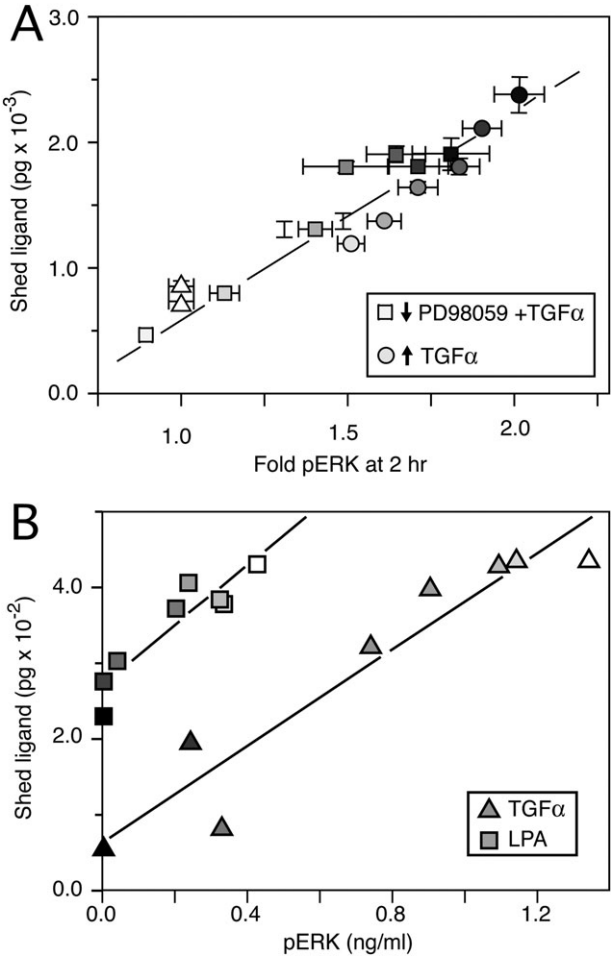

Fig. 5 Shedding is proportional to pERK levels. (A) Cells were incubated with increasing levels of TGFα (0.6 to 20 ng ml^{-1}) and the levels of pERK were measured at 2 hours using an in-cell western as described in Experimental. Ligand release was determined over 8 hours by ELISA and normalized to 10^6 cells. The amount of shed ligand is shown as a function of the observed levels of pERK (circles). Alternately, cells were pre-incubated with increasing concentrations of PD98059 (0.2–25 μM) for 30 minutes before stimulation with 20 ng ml^{-1} of TGFα (squares). Values from nonstimulated cells are triangles. Error bars represent standard deviation from triplicate wells. Increased shading indicates increasing concentrations of TGFα or decreasing concentrations of PD98059. (B) Differential effect of inhibiting MEK on TGFα and LPA-stimulated shedding. Data are the same as shown in Fig. 3A in which the effect of different concentration of U0126 on both ligand shedding and pERK levels were ascertained. LPA (0.5 μM; squares) or TGF (2.5 ng ml^{-1}; triangles) was added to cells treated with up to 10 μM U0126. The relationship between the levels of pERK and shed ligand observed at each concentration of U0126 is shown. Increasing darkness of symbols corresponds to increasing concentrations of U0126. All conditions are as described in Fig. 3A.

relative effect of the MEK inhibitor U0126 on both ligand shedding and pERK levels following either LPA or TGFα stimulation. As shown in Fig. 5B, the relationship between pERK levels and shed ligand as a function of U0126 is nearly linear for both LPA and TGFα-treated cells (regression coefficients of 0.93 and 0.95, respectively) with very similar slopes, indicating that the effect of pERK on shedding is agonist independent. However, in contrast to TGFα, only a small fraction of LPA-induced shedding was dependent on pERK activity. Thus, LPA stimulates ligand shedding not only directly, but also indirectly through ERK activation.

Our finding that key signaling nodes of the transactivation circuit display a linear relationship suggests that it could operate to arithmetically add multiple inputs. To test this hypothesis, we first examined the effect of adding increasing concentrations of HGF on both Ras and pERK activity. As shown in Fig. 6A, we found that the relationship between Ras activity and pERK levels following HGF stimulation was linear and similar in magnitude to that observed with TGFα (within 20%). The relationship between pERK levels stimulated by HGF and the shedding rate of TCT-NA was also linear (Fig. 6B). Furthermore, increasing rates of ligand

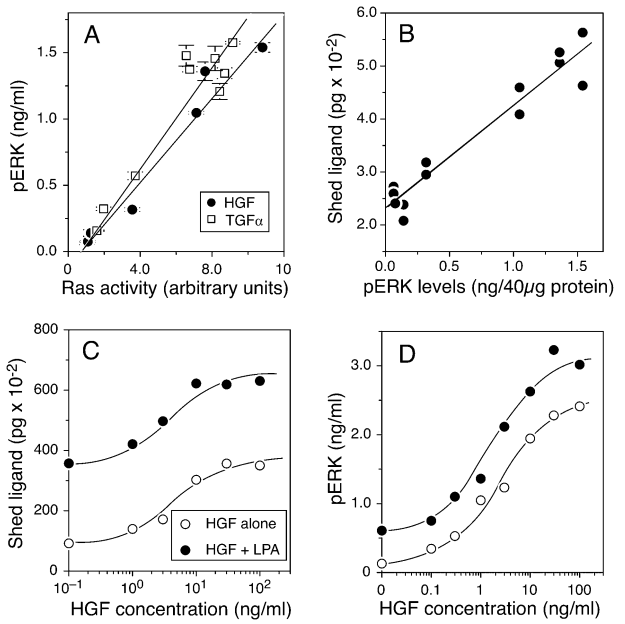

Fig. 6 ERK signals from LPA and HGF are additive through the transactivation circuit. (A) Cells were stimulated with TGFα (0.03–100 ng ml^{-1}) or HGF (0.3–100 ng ml^{-1}) for 5 minutes before collecting cell lysates for measuring the levels of activated Ras and pERK as described in Fig. 4b. Error bars represent standard deviation from triplicate samples. The lines are from linear regression. (B) Cells expressing TCT-NA were treated for 1 h with 225mAb to block the EGFR followed by the addition of different concentrations of HGF (0.1–100 ng ml^{-1}) for 1 h to measure ligand shedding or 15 min to measure pERK levels as described in Fig. 4a. (C) Cells were stimulated with HGF in either the presence or absence of a half-maximal dose of LPA (0.5 μM) for 1 h. The amount of immunoreactive EGF in the medium was then measured as described in Fig. 4a. (D) Cells were incubated with the indicated concentration of HGF in the presence (closed circles) and absence (open circles) of 0.1 μM LPA. The levels of activated ERK were measured by ELISA after 30 min as described in Experimental. Data are average of duplicate experiments.

shedding observed in response to increasing doses of HGF were additive to that induced by a fixed concentration of LPA (Fig. 6C). Likewise, the increased level of pERK stimulated by a fixed dose of LPA was additive to that stimulated by increasing concentrations of HGF (Fig. 6D). However, when cells were stimulated with a dose of HGF that induced a maximal level of pERK (> 100 ng ml^{-1}), the addition of LPA or TGFα did not significantly increase the observed levels of pERK (data not shown). These data demonstrate that at low doses of ligand, the transactivation circuit can arithmetically sum the activity of multiple signaling pathways at the level of pERK. The additive nature of ERK-stimulated and LPA-stimulated shedding (Fig. 5B and 6C) is also consistent with two distinct mechanisms of regulated shedding.

We have previously shown that the mitogenic response of cells to EGF is linearly proportional to ligand production,[31] but this is the first demonstration that this linearity can also be observed at the level of pERK. A variety of mechanisms could yield an effective linear behavior within these pathways. For instance, it has been proposed that formation of Ras nanoclusters in response to EGFR activation functions to linearize aspects of the Ras-ERK pathway.[32] In any event, a striking feature of this operating behavior is that at physiological ligand concentrations, the level of activated ERK becomes essentially a simple weighted sum of the diverse multiple inputs.

Modeling the EGFR transactivation circuit

To determine whether the circuit logic we have inferred from the behavior of the individual nodes operates in a quantitatively consistent manner overall, and to seek insights concerning circuit operation, we analyzed our experimental results using a simple systems engineering model. Although models for biochemical networks typically employ kinetic reaction-based equations representing detailed physicochemical processes,[33] the complete molecular mechanisms underlying our autocrine transactivation circuit are poorly understood, especially at the level of ligand shedding. Our objectives were better achieved by using a modular, ''block diagram'', model to represent the various input–output relationships and dynamic circuit processes. This approach is commonly used in dynamical systems modeling for applications involving poorly characterized internal mechanisms.[34]

Fig. 7 shows the block diagram for the system, which characterizes the flow of activity, or ''information'', in the circuit. Fig. 7A represents the regulatory topology in terms of general functional modules whereas Fig. 7B shows the system in terms of transfer functions. The system inputs and outputs were chosen based on the readouts in our experiments examining the dynamics of the transactivation circuit (Fig. 2). Our model contains five distinct core modules (large rectangles in the center of Fig. 7B) that describe the dynamics of ligand shedding and ERK activation. Each of these modules is linear and is characterized by a transfer function (TF) that describes how the module converts a time-dependent input, $I(t)$, to a time-dependent output, $O(t)$. The TF forms of the five core modules were chosen based on qualitative features seen in the experimental data in Fig. 2. The TF functional forms for the ligand shedding modules—module 1 (LPA-induced shedding) and module 2 (ERK-induced shedding)—were based on data from Fig. 2C. LPA-induced shedding was modeled as a transient increase in the shedding rate in response to a step change in the LPA concentration, whereas ERK-induced shedding was modeled as a time-delayed sustained increase in the shedding rate in response to a step change in ERK activity. TF functional forms for the ERK activation modules—modules 3 (autocrine ligand-induced pERK), 4 (exogenous TGFα-induced pERK), and 5 (HGF-induced pERK)—were based on the data in Fig. 2A. For these modules a step change in the ligand concentration was assumed to elicit a transient increase in ERK activity. The rise and decay times for ERK activation were assumed to be independent of the stimulus. Detailed descriptions of the various TF expressions and the rationale for their selection are presented in the ESI.†

Core modules 2 (ERK-induced shedding) and 3 (autocrine ligand-induced pERK) together describe a positive feedback loop, and the system inputs feed into this loop by contributing independently to either ligand shedding (LPA) or ERK activation (TGFα and HGF). Based on our experimental

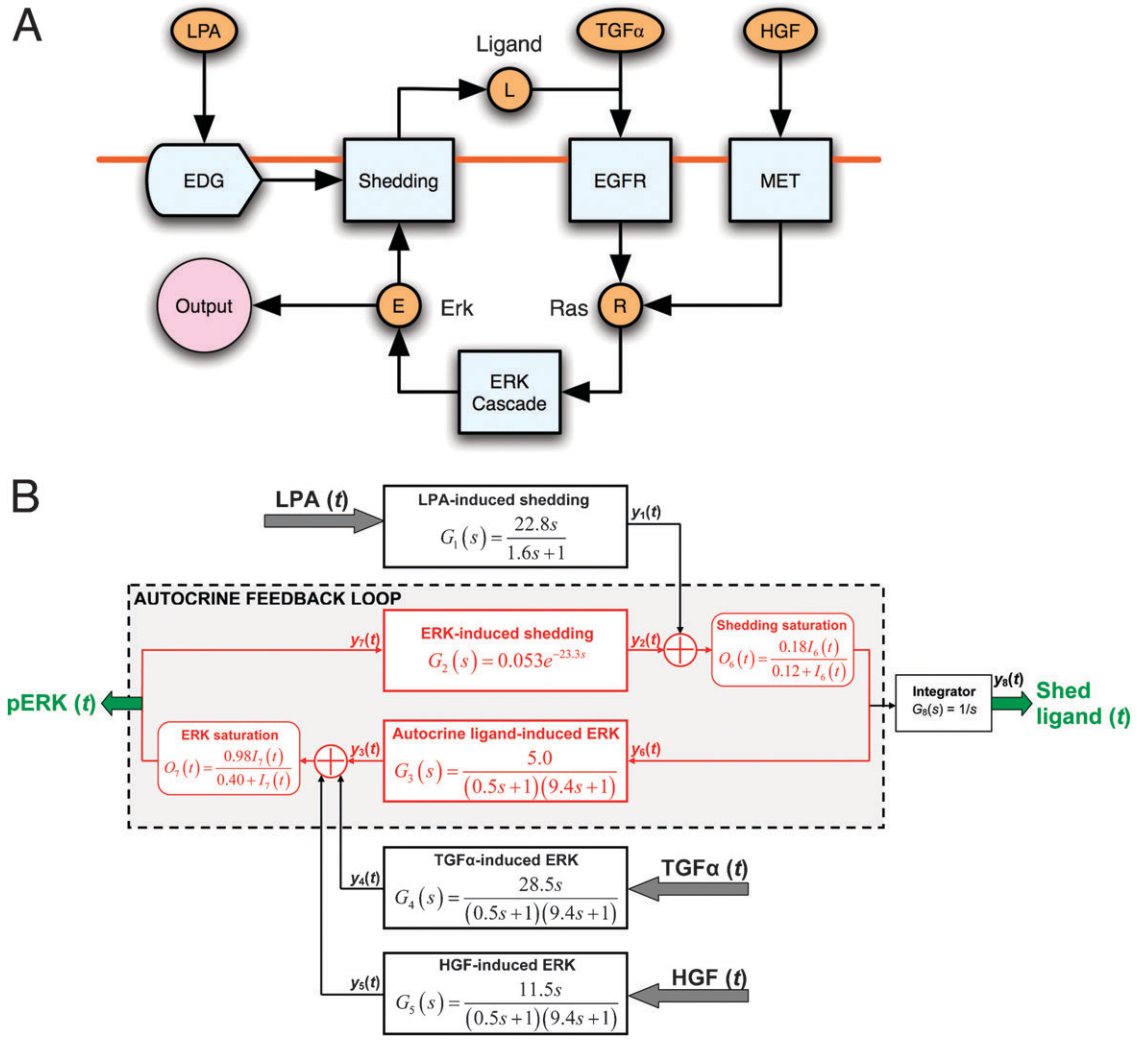

Fig. 7 Model for the transactivation circuit. (A) Regulatory topology in terms of functional modules. The inputs are LPA, TGFα and HGF working through their respective receptors (EDG, EGFR or MET). The nodes measured in this study are indicated by circles. (B) Mathematical model in terms of transfer functions. The model consists of five core linear modules (large rectangles). The input–output characteristics of these modules are determined by the transfer functions (TFs) shown with the boxes. Module numbering is reflected in the TF expression and the output variable for each module. An 's' in the numerator of the TF (modules 1, 4 and 5) indicates an adaptive response—a step input results in a transient output. A term of type '$e^{-t_d s}$' (module 2) indicates that the module responds to the input after a dead-time of t_d minutes. Terms of type '$\tau s + 1$' in the denominator (modules 1, 3–5) capture the sluggishness of the response. The overall ligand shedding rate is a sum of the shedding rates induced by LPA (y_1) and ERK activity (y_2). The overall ERK activity is the sum of the ERK activities induced by autocrine ligand (y_3), TGFα (y_4), and HGF (y_5). The net shedding rate and ERK activity are modified using the static saturation filters shown in modules 6 and 7 respectively (rounded rectangles). The ligand shedding rate is integrated by module 8 to yield the total amount of shed ligand. The structure of the model and the TF functional forms were chosen based on the qualitative features of ERK and ligand shedding dynamics observed in our experiments. Parameters indicated within the modules were determined by fitting the model outputs simultaneously to all of our time-course and dose response experiments.

observations, we assumed that the overall ligand shedding rate (and pERK level) is a sum of the direct contribution from LPA (TGFα and HGF for p-ERK) and the indirect contribution from the feedback loop itself. Linear additivity is captured using "adders" for ligand shedding and pERK in our mathematical model (circles in Fig. 7B). Since ligand shedding and ERK activation are saturable processes, we included static saturation filters for the overall shedding rate and pERK levels to ensure that these quantities stay bounded in the mathematical model (rounded rectangles in Fig. 7B). We integrated the ligand shedding rate over time (module 8) to determine the total amount of shed ligand at any given time point.

Given the input doses of LPA, TGFα and HGF (the magnitude of the step inputs for these quantities), the model generates values for outputs *pERK*(*t*) and *Shed ligand*(*t*). Information about the TF parameters is available from the dynamics experiments shown in Fig. 2A and C, while information about shedding and pERK saturation is available from the dose response experiments in Fig. 4A and B, 6C and D. We estimated the TF and saturation parameters of the model by simultaneously fitting it to all of the dynamics and dose response data sets. We performed 100 parameter estimation runs starting at random points within the ranges specified for each of the model parameters. We analyzed all solutions that

yielded a comparably good fit between model predictions and experimental data to determine possible correlations between the parameters and to quantify parameter uncertainty (Table S3, ESI†). The gain terms of modules 1 and 2 and the half-maximal saturation term of module 6 were mutually correlated. These parameters together determine the magnitude of ligand shedding. Similarly, the gain terms of modules 3, 4 and 5 and the half-maximal saturation term of module 7 formed a correlated set, which together determine the magnitude of ERK activation. Due to these correlations, each of these parameters had a coefficient of variation (CV = standard deviation/mean) between 0.25 and 0.3. The common parameter that determines the rise time for ERK activation in modules 3, 4 and 5 also had a CV in this range due to the lack of early time point data to accurately estimate this parameter. All other parameters had CV values less than 0.1 and were thus estimated with good confidence. The parameter set that yielded the best fit between model predictions and the experimental data is presented in Fig. 7B and is used in all subsequent analyses. Despite the uncertainties in the individual parameters, our predictions for the overall behavior of the transactivation circuit would remain essentially unchanged when we use any of the parameter sets that yield a good match between model and experiment (Fig. S7, ESI†).

Despite being forced to simultaneously explain 6 distinct time courses and 5 distinct dose response data sets, the model does a good job of fitting the data (R^2 values are greater than 0.82 for all of the data sets except for the HGF-induced shedding dose response for which $R^2 = 0.51$). Thus, the model is internally self-consistent and is suitable for characterizing the general behavior of the autocrine circuit. (More details on model construction and parameter estimation are provided in the ESI†, including Tables S2, S3 and Fig. S5–S7.)

To characterize the stability of the transactivation circuit, we computed the system steady states and analyzed the behavior of the dynamic system in the vicinity of these steady states using linear analysis (ESI†). For these calculations, we used the steady-state pERK level as the system readout, and varied the strength of the positive feedback loop by varying the gain of the ERK-induced shedding module (parameter K_2). K_2 captures the strength of the coupling from ERK activation to ligand shedding. For $K_2 < 0.11$, the system has a single stable steady at pERK = 0 (Fig. 8A). Under these conditions, stimulating the circuit transiently results in a transient pERK response that decays to zero. Although we have positive feedback in the system, the feedback loop is not strong enough to induce sustained activity. However for $K_2 > 0.11$, the steady-state at pERK = 0 loses its stability (dotted line in Fig. 8A), and we instead have a stable steady-state at a value of pERK that depends upon the strength of the feedback loop. Under these conditions, with an initial pERK value of 0, any transient perturbation would result in a sustained, submaximal, level of ERK activity.

Based on our experimental data we estimate a K_2 value of 0.053 for HMECs, for which the stable steady-state is at $pERK^{ss} = 0$. To determine whether this feedback strength is sufficient to modulate the response dynamics, we examined the pERK response to a physiological concentration of TGFα (100 pg ml^{-1} [31]) in the absence ($K_2 = 0$) and presence ($K_2 = 0.053$) of feedback (Fig. 8B). In the absence of feedback, the pERK response decays to 0 by ~50 min (Fig. 8B, dotted line). This is a consequence of the negative feedback mechanisms that turn off ERK activation. Such shut-off mechanisms are implicitly encoded in the TF for exogenous ligand-induced ERK activation, where ERK activation is represented as a transient process even though the input is a step change in ligand concentration. The positive feedback due to autocrine ERK activation has a significant effect on pERK dynamics (Fig. 8B, solid line). Although the response would eventually decay to 0, the feedback loop is strong enough to amplify and prolong the effects of the initial TGFα stimulus.

To further illustrate the amplifying effect of the autocrine feedback loop we consider a scenario where TGFα and HGF rather than transiently activating the circuit, make sustained contributions to ERK activation (Fig. 8C). In a transactivation circuit without autocrine feedback the net steady-state ERK output would simply be the sum of the contributions from these two stimuli (dotted lines in Fig. 8C). Note that the levels of ERK activation considered here are relatively low, and the system is not saturated. As seen in Fig. 8C, even the modest feedback strength in our system is sufficient to amplify the response, and results in an ERK output that is higher than the sum of the TGFα and HGF contributions (Fig. 8C compares solid lines with dotted lines). The strength of the feedback loop will depend on the ability of the shed ligand to be captured by the EGFR, which depends on the extracellular environment.[35] Thus the transactivation circuit, by virtue of the autocrine feedback loop, acts as a context-dependent amplifier of stimuli that activate the circuit.

To examine the effect of the feedback strength on pERK dynamics we altered the K_2 value in simulations where the circuit was activated using 100 pg ml^{-1} TGFα (Fig. 8D). As expected, a K_2 value of 0.05, which is below the threshold of 0.053, results in a transient ERK activation response starting from a pERK value of 0 (bottom solid line). As the feedback strength is increased beyond the threshold value, the steady-state at pERK = 0 becomes unstable. Under these conditions, even prior to ligand addition, the system is expected to have an elevated level of ERK activity. At the higher gain values, we again see a transient ERK response, but the response starts from an elevated steady-state and returns to it (top two solid lines in Fig. 8D). The fact that irrespective of the strength of the feedback we return to the initial steady-state is a reflection of negative feedback mechanisms that shut off ERK activity within the feedback loop. This feature is implicitly encoded in our mathematical model in the form of the assumption that an impulse in the autocrine ligand shedding rate (a step change in shed ligand concentration) would result in a transient pERK response. If not for this feature, the system steady-state would always be unstable and any perturbation would result in a maximal pERK response. Our results also indicate that as we increase the feedback strength, rather than achieving increased amplification of external stimuli, we end up with a higher basal activity, and reduced responsiveness (Fig. 8D). This model prediction is in agreement with our previous experimental observations on the effect of changing autocrine ligand expression on pERK dynamics.[20]

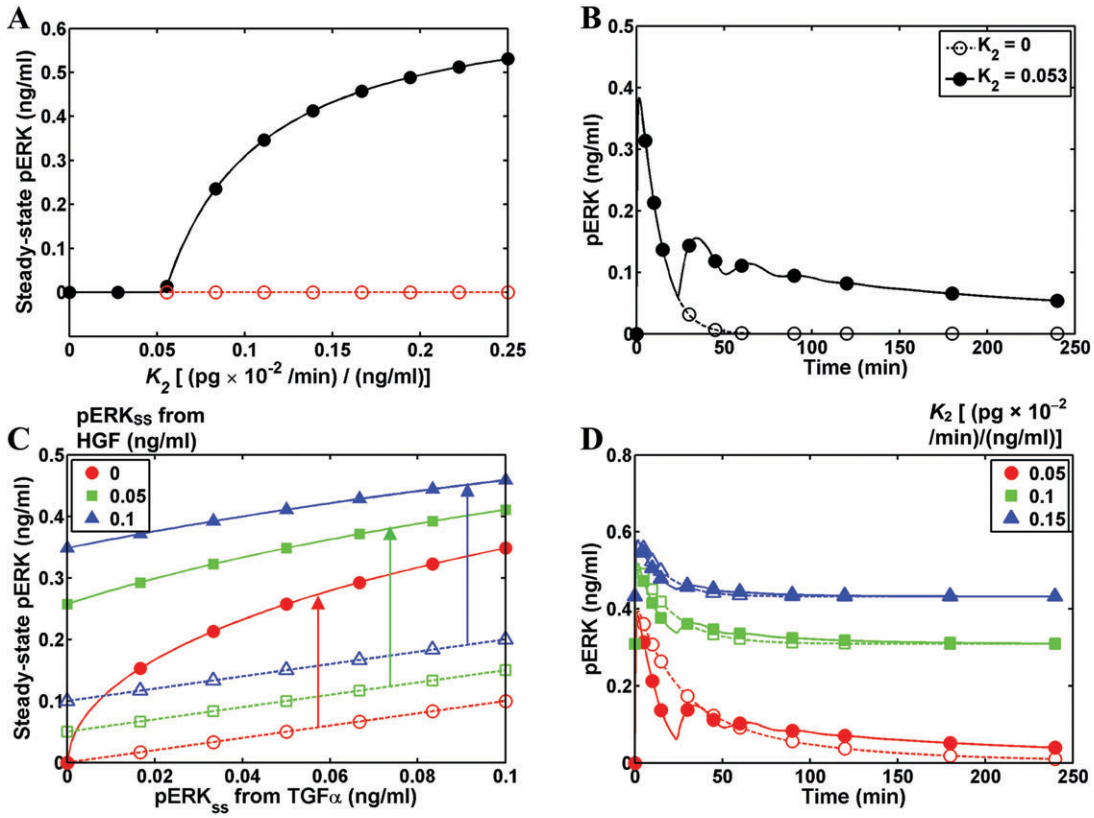

Fig. 8 Dynamic behavior of the transactivation circuit. For the calculations shown in all panels, parameters were held at the values shown in Fig. 7 unless specified otherwise. (A) Steady-state pERK levels were computed for the autocrine feedback loop, and are plotted as function of K_2 (the gain of the ERK-induced shedding module). The stable steady state is depicted using a solid line with filled circles. The dotted line with open circles indicates the unstable steady state at pERK = 0. (B) The pERK output of the transactivation circuit in response to 100 pg ml^{-1} TGFα is plotted as a function of time in the absence (dotted line) and presence (solid line) of autocrine feedback. (C) The steady-state pERK output of the transactivation circuit (solid lines, filled circles) is plotted for cases where TGFα and HGF make sustained contributions to ERK activity at the levels specified in the *x*-axis and the legend respectively. Dotted lines and open markers indicate the expected steady-state pERK output in the absence of the autocrine feedback loop. Arrows are presented to enable comparison between corresponding cases with and without feedback. (D) The pERK output of the transactivation circuit in response to 100 pg ml^{-1} TGFα is plotted as a function of time in the absence (dotted lines and open markers) and presence (solid lines and filled markers) of a time delay in ERK-induced shedding. Results are shown for the three different values of feedback gain K_2 indicated in the legend.

Finally, we used the model to explore the operational significance of the time-delay that we observed between activation of ERK and subsequent ligand shedding. The pERK dynamics in the absence of this time delay is presented as dotted lines with open markers in Fig. 8D. When these results are compared with the respective simulations which include the delay (solid lines with closed markers), we find that the delay does not significantly affect the response. The system steady-state remains unchanged, but the delay causes a time shift with a slight increase in the time taken to reach steady state.

Our simulations show that the positive autocrine feedback through ERK will act as an amplifier of the original signal, depending on its "gain", or the coupling between ERK-induced shedding and subsequent EGFR binding. Thus, any particular initial stimulus will generate an ultimate downstream signal based not only on that generated directly by the individual cue but also influenced by extracellular conditions that modulate autocrine ligand/EGFR binding.[36–38] Consistent with this idea, we recently demonstrated that HGF-stimulated proliferation in HMEC is additive to that mediated by context-dependent autocrine signaling.[25]

Positive feedback through an ultrasensitive regulatory step, such as the ERK pathway, can result in bistability and irreversible switching to a maximal level of ERK activity beyond a threshold level of stimulation.[39] However, our simulations predict that the transactivation circuit behaves as a stable context-dependent amplifier. The circuit is stable in an inactive state (pERK ≈ 0) in that any stimulus in this state elicits a transient pERK response that decays back to the inactive state. Above a critical value of the feedback strength, the circuit maintains a non-zero basal steady state level of pERK that depends on the gain, but still continues to respond in a transient fashion. These predictions are confirmed by our recent data on the effect of expressing different levels of autocrine ligands, which effectively increases the gain in the transactivation circuit.[20] We found that compared to parental cells, ligand over-expressing cells had a higher basal ERK

activity, and under 'acute' exogenous ligand treatment (addition of 2 nM EGF) showed a smaller pERK response with a faster return to the basal state. Further, when we blocked the feedback loop in the ligand-expressing cells with the EGFR blocking antibody mAb225, pERK levels dropped to 0, but returned to the elevated steady state levels within 2 hours of antibody removal.[20] Our model suggests that this stability to external perturbations is a consequence of the adaptive mechanisms that turn off ERK signaling, and enables ERK to respond to changes in ligand concentration as opposed to the absolute level of ligand.

Conclusions

The aim of our study was to elucidate the logic of EGFR transactivation by disparate stimuli to understand how information from multiple inputs is combined to control downstream signal transduction. We have demonstrated that transactivation includes a positive feedback circuit that connects proteolytic release of autocrine TGFα to EGFR binding to Ras-mediated ERK signaling, and that the activity of this circuit can be regulated at different points by diverse inputs. Some of our findings confirm previous isolated reports, but our investigation served to unify and extend a substantial body of previous literature reporting various facets of the overall circuit from a wide spectrum of biological settings.[1–5] Although we have focused our efforts here on LPA and HGF as non-EGFR-binding stimuli, along with TGFα as the connecting EGFR-binding autocrine ligand that stimulates its own release, we anticipate that other EGFR transactivating stimuli such as mechanical force, extracellular matrix components, hormones, and small peptide GPCR-binding ligands could intersect this circuit at appropriate locations as well.

One central biological insight from our findings is that the diverse entry loci of the transactivation circuit permits disparate stimuli to be integrated into the net ERK pathway signal with quantitatively calibrated degrees. That is, even though LPA and HGF both induce the Ras–ERK pathway, they do so *via* different points along the recursive TGFα–EGFR–Ras–ERK circuit. Accordingly, similar dynamic inputs of LPA and HGF will yield non-identical ERK outputs so their contributions to cell functional behavior can be relatively greater or lesser even though the action of both might occur through ERK-mediated effectors. Different growth factors (*e.g.*, NGF *versus* EGF) can induce disparate cell phenotypes despite both acting *via* the ERK pathway because of their ability to elicit quantitatively diverse ERK dynamics.[40–42] Our EGFR transactivation circuit here obviously allows similar opportunity for dynamically encoded ligand specificities, but the recursive nature of this circuit results in the "real-time feedback interrogation" of the cellular environment.

As we tackle larger and more complex problems in systems biology, we will inevitably have to deal with scenarios where the internal mechanisms of a system are not completely known, but we still desire insights into system behavior from a limited set of observations. The black-box systems engineering modeling approach employed here can prove to be extremely useful in this regard. It enables us to cast our hypotheses about the system into quantitative terms and test whether they are consistent with the experimental data. The use of transfer functions enables us to model the dynamics of individual system modules, and investigate the effect of the coarse-grained network topology and of particular dynamic properties on the higher order behavior of the system. Such black-box approaches are very useful as a starting point for the hierarchical investigation of a poorly characterized biological system because they can identify critical dynamic features of a system that should be targeted for further experimental investigations. For instance, we find that the transactivation circuit owes its stability to the adaptive mechanisms that turn off ERK signaling. Thus, although we know of multiple negative feedback mechanisms in the ERK signaling cascade that potentially could be responsible, further work on defining the most important of these adaptation mechanisms is still needed. In addition, understanding the factors that modulate autocrine gain will be crucial in delineating the mechanisms by which cells detect their extracellular context.

Experimental

Antibodies and inhibitors

Rabbit polyclonal anti-EGFR (1005) was obtained from Santa Cruz Biotechnology. Anti-AKT (Pan), anti-phospho-AKT (Ser473), anti-ERK, and anti-phospho-p44/42 MAP Kinase (Thr202/Tyr204) (E10) antibodies were obtained from Cell Signaling Technology. Goat anti-rabbit and goat anti-mouse horseradish peroxidase conjugated antibodies were obtained from Jackson Immunoresearch Laboratories. LPA, U-0126, Wortmannin, LY294002 and PP2 were purchased from BIOMOL Research Laboratories Inc. PD98059 was purchased from BIOMOL Research Laboratories Inc. SB203580 was from Calbiochem and gefitinib from WuXi PharmaTech, Shanghai, China. Batimastat (BB-94; [4-(*N*-hydroxyamino)-2*R*-isobutyl-3*S*-(thienylthiomethyl)succinyl]-L-phenylalanine-*N*-methylamide) was custom synthesized by Kimia Corporation (Santa Clara, CA). All other inhibitors were from BIOMOL Research Laboratories Inc. Hepatocyte growth factor/scatter factor (HGF), EGF, and TGFα were from Peprotech, Inc. The receptor blocking anti-EGFR 225 monoclonal antibody was isolated from a hybridoma cell line obtained from the American Type Culture Collection. Anti-EGF antibodies for the EGF ELISA include 236 (R&D Systems) and a rabbit polyclonal described previously.[43] The tertiary ELISA detection antibody was an alkaline phosphatase-conjugated goat anti-rabbit antibody (Sigma).

Cell line and culture

The human mammary epithelial cell (HMEC) line 184A1 was obtained from Martha Stampfer (Lawrence Berkeley National Laboratory) and maintained in DFCI-1 media as previously described.[44] Serum-free media consisted either of DFCI-1 complete media lacking fetal bovine serum, bovine pituitary extract, and EGF supplements (SFM medium) or alpha:MEM-F12 medium containing 0.1% BSA, 10 mM HEPES (DFB medium) as noted. Cells were incubated for

16 h in serum-free media before starting each experiment. All experiments were performed using cells within 15 passages of thawing.

Construction and expression of ligand chimeras

The TCT ligand chimera was constructed as previously described.[20] To construct the "no affinity" (NA) derivative, a point mutation was introduced into the EGF portion of the molecule to change leucine 15 to glutamic acid using the following primers: forward primer: 5′-CAC GAC GGG TAC TGC **GAG** CAC GAC GGT GTT TGC-3′; reverse primer: 5′-GCA AAC ACC GTC GTG **CTC** GCA GTA CCC GTC GTG-3′. Mutagenesis was accomplished using the Stratagene Quik Change Mutagenesis kit and the parental ligand chimera. Cells were retrovirally transduced with the TCT and TCT-NA constructs as previously described.[20]

Ligand release assays

Cells were plated in DFCI-1 medium 350 000 cells per well in 6-well plates or 60 000–80 000 cells per well in 12-well plates on day 1 and switched to DFB or SFM medium on day 2. After 16 h the cells were rinsed in fresh medium and then 1 ml of medium alone or containing the indicated inhibitors or stimuli was added to each well. Inhibitors were generally added 30–60 min prior to the initiation of the experiment (as indicated in the figure legends). Media samples were collected at the indicated times, clarified by centrifugation at 1000 or 14 000 rpm and then immediately frozen at −20 °C or analyzed by EGF ELISA as previously described.[43] For determination of amphiregulin levels, medium was collected from each dish, clarified by centrifugation and then analyzed directly for amphiregulin using the AR ELISA kit from R&D Systems.

Phospho-ERK assays

In most experiments, pERK levels were measured in cell lysates using phospho-ERK1 (T202/Y204) sandwich ELISA kits from R&D Systems in a 96-well format with slight modifications. Briefly, protein was isolated from HMEC using MTG lysis buffer provided with the kit. Approximately 40 μg of total protein was diluted to a 1 : 1 ratio with a lysis buffer supplemented with 8 M urea. The lysate samples were vortexed and incubated at room temperature for 1 h and then centrifuged at 2000 × *g* for 5 min, and the supernatant was collected in a fresh tube. The samples were diluted to a final urea concentration of 1 M. Protein concentrations were measured in each sample using the BCA assay kit from Pierce Chemical Co. ELISA assays were typically done in triplicate for each sample and the results corrected for protein concentration, using 40 μg as the per-sample standard.

In some experiments, ERK phosphorylation was measured using the in-cell western blot with the Odyssey system (LI-COR). Cells were plated in 96-well plates (Nunc) at a density of 20 000 cells per well for experiments. Following specific treatments, cells were fixed with formaldehyde (4% in PBS) for 20 min at room temperature, permeabilized in 0.1% triton in PBS and blocked with Odyssey Blocking Buffer (LI-COR) 1 : 1 in PBS (OBB). Cells were stained for ERK 1/2 phosphorylation on Thr202 and Tyr204 (1 : 100 in OBB) overnight at 4 °C. IRDye 800 anti-rabbit IgG (1 : 800 in OBB) was used as the secondary antibody. Plates were washed 3× with 0.1% Tween 20 in PBS between each antibody incubation and prior to scanning. Plates were scanned using the Odyssey system (LI-COR). The integrated intensity of each well was normalized to untreated wells on the same plate to show normalized fold ERK phosphorylation at each time point under each condition.

When screening inhibitors for their effect on agonist-induced ERK phosphorylation, the Luminex assay system was used. Briefly, cells were grown to approximately 80% confluency in 24-well plates and treated with inhibitors for 30 min before adding agonists for 5–10 min. Cells were rinsed in ice-cold saline and lysed in 150 μl of Beadlyte™ Cell Signaling Universal Lysis Buffer (Millipore Corporation) for 10 min on ice. The lysates were transferred to fresh microtiter plates, clarified by centrifugation. 10 μl of lysate was incubated overnight with 25 μl of Beadlyte™ Anti-Erk/MAP Kinase 1/2 Beads in 96-well filter plates and pERK was detected using biotinylated anti-phospho-Erk 1/2 (Thr185/Tyr187) according to the manufactures' protocol. The relative levels of pERK were then determined using a Luminix 100 instrument and normalized to the level of pERK observed in the absence of inhibitors.

Other quantitative assays

The levels of phosphorylated EGFR were measured using the lysates prepared as described above for the pERK ELISA assay. The STAR phospho-EGFR ELISA kit from Millipore was used, following the manufacturer's instructions. The levels of activated Ras were determined by using a pull-down assay kit based on the Raf–RBD–GST fusion protein from Cytoskeleton, Inc.[45] In brief, cells were rinsed and lysed in detergent solution containing a protease inhibitor cocktail (provided with kit). A cell scraper was used to transfer the cells to a microcentrifuge tube and the lysate was clarified by centrifugation. Approximately 500 μg of total protein was incubated with 15 μg Raf1–RBD beads for 1 h at 4 °C on a rotator. The beads were rinsed with a wash buffer twice, suspended in SDS sample buffer, heated to 95 °C for 5 min and then run on a 12% SDS gel and transferred to polyvinylidene difluoride membrane, and probed with an anti-Ras antibody. Horseradish peroxidase-conjugated goat anti-mouse secondary antibody was used at 1 : 5000 dilution. Quantification of bands was performed using a Boehringer-Mannheim LumiImager and associated image analysis software.

Computational model of EGFR transactivation

We constructed a mathematical model to analyze our experimental results for ERK activation and ligand shedding dynamics in response to LPA, TGFα and HGF. The model was written in MATLAB and is available on request. Detailed descriptions of the steps involved in model construction and parameter estimation are provided in the ESI.† Briefly, we developed a block diagram representation for the system based on the logic of the EGFR transactivation system deduced in this manuscript. We defined the system as containing five

distinct core modules that are involved in determining the dynamics of ligand shedding and ERK activation. As a simplifying assumption, each of these modules was modeled as a linear dynamic system, and its input–output relationship was represented using a transfer function. Parsimonious transfer function forms were chosen for each of the modules based on the qualitative features of ERK and ligand shedding dynamics measured in the experiments. These modules were connected to reflect the additivity in ERK activation and ligand shedding seen in our experiments. Saturation filters were included to ensure that the ligand shedding rate and pERK levels stay bounded within the maximal values determined in the experiments. The governing equations for the model were expressed in the time domain in the form of a set of delay-differential equations. The model was then simultaneously fit to the entire experimental dynamics and dose response data sets for ERK activation and ligand shedding in response to the three distinct stimuli in order to estimate the TF and saturation parameters (see ESI†). We defined search ranges for each of the parameters and performed 100 optimization iterations starting from random positions within the chosen parameter bounds. The root-mean-squared deviation (RMSD) between the model predictions and the experimental data was determined for each of these solutions. Parameter sets that yielded an RMSD within 1% of the minimum value were analyzed to determine the uncertainty in each of the individual parameters (Table S3, ESI†). The best-fit parameter set that resulted in the lowest RMSD was used to obtain the results in Fig. 7 and 8. Once the model was parameterized as above, we examined the consequences of varying specific parameters on the system steady-states and dynamics. In these studies, the chosen parameters were varied in the specified range, while the rest of the parameters were held fixed at the values obtained from the parameter optimization.

Abbreviations

EGF	epidermal growth factor
EGFR	epidermal growth factor receptor
ELISA	enzyme-linked immunosorbent assay
ERK	extracellular signal regulated kinase
HGF	hepatocyte growth factor
HMEC	human mammary epithelial cell
LPA	lysophosphatidic acid
MEK	MAP–ERK kinase
pERK	phosphorylated form of ERK
TCT	TGFα cytoplasmic tail fused to EGF
TCT-NA	TCT no affinity form
TGFα	transforming growth factor alpha
TF	transfer functions

Acknowledgements

This work was funded by the Biomolecular Systems Initiative LDRD Program at the Pacific Northwest National Laboratory; a multiprogram national laboratory operated by Battelle for the U.S. Department of Energy under Contract DE-AC05-76RL01830, and by NIH grants CA96504 to DAL, and by a Whitaker Foundation Graduate Fellowship to EJJ. The authors thank Noah Pefaur for technical assistance and Karin Rodland for many useful discussions.

References

1 N. E. Bhola and J. R. Grandis, *Front. Biosci.*, 2008, **13**, 1857–1865.
2 A. Citri and Y. Yarden, *Nat. Rev. Mol. Cell Biol.*, 2006, **7**, 505–516.
3 O. M. Fischer, S. Hart, A. Gschwind and A. Ullrich, *Biochem. Soc. Trans.*, 2003, **31**, 1203–1208.
4 N. Prenzel, O. M. Fischer, S. Streit, S. Hart and A. Ullrich, *Endocr. Relat. Cancer*, 2001, **8**, 11–31.
5 E. Zwick, P. O. Hackel, N. Prenzel and A. Ullrich, *Trends Pharmacol. Sci.*, 1999, **20**, 408–412.
6 S. J. Fuller, K. Sivarajah and P. H. Sugden, *J. Mol. Cell. Cardiol.*, 2008, **44**, 831–854.
7 J. M. Jacobs, K. M. Waters, L. E. Kathmann, D. G. Camp, 2nd, H. S. Wiley, R. D. Smith and B. D. Thrall, *J. Proteome Res.*, 2008, **7**, 558–569.
8 I. Kuwahara, E. P. Lillehoj, W. Lu, I. S. Singh, Y. Isohama, T. Miyata and K. C. Kim, *Am. J. Physiol.: Lung Cell. Mol. Phys.*, 2006, **291**, L407–L416.
9 E. Rozengurt, *J. Cell. Physiol.*, 2007, **213**, 589–602.
10 H. M. Shepard, C. M. Brdlik and H. Schreiber, *J. Clin. Invest.*, 2008, **118**, 3574–3581.
11 G. Carpenter, *Science's STKE*, 2000, **2000**, 1pe.
12 R. C. Harris, E. Chung and R. J. Coffey, *Exp. Cell Res.*, 2003, **284**, 2–13.
13 A. B. Singh and R. C. Harris, *Cell. Signalling*, 2005, **17**, 1183–1193.
14 F. L. Roudabush, K. L. Pierce, S. Maudsley, K. D. Khan and L. M. Luttrell, *J. Biol. Chem.*, 2000, **275**, 22583–22589.
15 S. A. Tomlins, N. Bolllinger, J. Creim and K. D. Rodland, *Exp. Cell Res.*, 2005, **308**, 439–445.
16 H. Fan and R. Derynck, *EMBO J.*, 1999, **18**, 6962–6972.
17 Z. Gechtman, J. L. Alonso, G. Raab, D. E. Ingber and M. Klagsbrun, *J. Biol. Chem.*, 1999, **274**, 28828–28835.
18 T. Umata, M. Hirata, T. Takahashi, F. Ryu, S. Shida, Y. Takahashi, M. Tsuneoka, Y. Miura, M. Masuda, Y. Horiguchi and E. Mekada, *J. Biol. Chem.*, 2001, **276**, 30475–30482.
19 M. R. Stampfer, C. H. Pan, J. Hosoda, J. Bartholomew, J. Mendelsohn and P. Yaswen, *Exp. Cell Res.*, 1993, **208**, 175–188.
20 E. J. Joslin, L. K. Opresko, A. Wells, H. S. Wiley and D. A. Lauffenburger, *J. Cell Sci.*, 2007, **120**, 3688–3699.
21 B. H. Will, D. A. Lauffenburger and H. S. Wiley, *Tissue Eng.*, 1995, **1**, 83–96.
22 J. Dong, L. K. Opresko, P. J. Dempsey, D. A. Lauffenburger, R. J. Coffey and H. S. Wiley, *Proc. Natl. Acad. Sci. U. S. A.*, 1999, **96**, 6235–6240.
23 J. Baselga, J. Mendelsohn, Y. M. Kim and A. Pandiella, *J. Biol. Chem.*, 1996, **271**, 3279–3284.
24 K. Nandagopal, D. K. Tadaki, J. A. Lamerdin, E. H. Serpersu and S. K. Niyogi, *Protein Eng.*, 1996, **9**, 781–788.
25 K. D. Rodland, N. Bollinger, D. Ippolito, L. K. Opresko, R. J. Coffey, R. Zangar and H. S. Wiley, *J. Biol. Chem.*, 2008, **283**, 31477–31487.
26 S. M. Soond, B. Everson, D. W. Riches and G. Murphy, *J. Cell Sci.*, 2005, **118**, 2371–2380.
27 O. Halevy and L. C. Cantley, *Exp. Cell Res.*, 2004, **297**, 224–234.
28 C. R. Maroun, M. A. Naujokas, M. Holgado-Madruga, A. J. Wong and M. Park, *Mol. Cell. Biol.*, 2000, **20**, 8513–8525.
29 T. Sasaoka, W. J. Langlois, J. W. Leitner, B. Draznin and J. M. Olefsky, *J. Biol. Chem.*, 1994, **269**, 32621–32625.
30 J. M. Haugh, A. C. Huang, H. S. Wiley, A. Wells and D. A. Lauffenburger, *J. Biol. Chem.*, 1999, **274**, 34350–34360.
31 A. E. DeWitt, J. Y. Dong, H. S. Wiley and D. A. Lauffenburger, *J. Cell Sci.*, 2001, **114**, 2301–2313.
32 T. Tian, A. Harding, K. Inder, S. Plowman, R. G. Parton and J. F. Hancock, *Nat. Cell Biol.*, 2007, **9**, 905–914.
33 B. B. Aldridge, J. M. Burke, D. A. Lauffenburger and P. K. Sorger, *Nat. Cell Biol.*, 2006, **8**, 1195–1203.
34 A. V. Oppenheim, A. S. Willsky and S. H. Nawab, *Signals and Systems*, Prentice-Hall, 1997.

35 M. Pribyl, C. B. Muratov and S. Y. Shvartsman, *Biophys. J.*, 2003, **84**, 3624–3635.
36 B. D. Cosgrove, C. Cheng, J. R. Pritchard, D. B. Stolz, D. A. Lauffenburger and L. G. Griffith, *Hepatology*, 2008, **48**, 276–288.
37 K. A. Janes, S. Gaudet, J. G. Albeck, U. B. Nielsen, D. A. Lauffenburger and P. K. Sorger, *Cell (Cambridge, Mass.)*, 2006, **124**, 1225–1239.
38 S. Y. Shvartsman, M. P. Hagan, A. Yacoub, P. Dent, H. S. Wiley and D. A. Lauffenburger, *Am. J. Physiol. Cell Physiol.*, 2002, **282**, C545–C559.
39 O. Brandman and T. Meyer, *Science*, 2008, **322**, 390–395.
40 S. D. Santos, P. J. Verveer and P. I. Bastiaens, *Nat. Cell Biol.*, 2007, **9**, 324–330.
41 S. Traverse, N. Gomez, H. Paterson, C. Marshall and P. Cohen, *Biochem. J.*, 1992, **288**(Pt 2), 351–355.
42 D. Vaudry, P. J. Stork, P. Lazarovici and L. E. Eiden, *Science*, 2002, **296**, 1648–1649.
43 H. S. Wiley, M. F. Woolf, L. K. Opresko, P. M. Burke, B. Will, J. R. Morgan and D. A. Lauffenburger, *J. Cell Biol.*, 1998, **143**, 1317–1328.
44 V. Band and R. Sager, *Proc. Natl. Acad. Sci. U. S. A.*, 1989, **86**, 1249–1253.
45 J. de Rooij and J. L. Bos, *Oncogene*, 1997, **14**, 623–625.

